

## Research Article

# In Vivo Corrosion Behavior of Biodegradable Magnesium Alloy by MAF Treatment

Xinzhe Gao <sup>1</sup>, Chun Yu Dai, <sup>1</sup> Qi Jia <sup>1</sup>, ChuanYao Zhai, <sup>1</sup> HaoYu Shi <sup>1</sup>, Yifan Yang, <sup>1</sup> Bing Cheng Zhao <sup>1</sup>, HongXin Cai <sup>1</sup>, Eui-Seok Lee <sup>2</sup>, and Heng Bo Jiang <sup>1</sup>

<sup>1</sup>The Conversationalist Club, School of Stomatology, Shandong First Medical University & Shandong Academy of Medical Sciences, Tai'an, Shandong 271016, China

<sup>2</sup>Department of Oral and Maxillofacial Surgery, Graduate School of Clinical Dentistry, Korea University, Seoul 02841, Republic of Korea

Correspondence should be addressed to Eui-Seok Lee; [ees225@hanmail.net](mailto:ees225@hanmail.net) and Heng Bo Jiang; [hengbojiang@vip.qq.com](mailto:hengbojiang@vip.qq.com)

Received 26 January 2021; Accepted 23 April 2021; Published 4 May 2021

Academic Editor: Lavinia C. Ardelean

Copyright © 2021 Xinzhe Gao et al. This is an open access article distributed under the Creative Commons Attribution License, which permits unrestricted use, distribution, and reproduction in any medium, provided the original work is properly cited.

Coating treatment plays an irreplaceable role in propelling the clinical application of magnesium alloys. This experiment was designed in order to observe the anticorrosion behavior of magnesium fluoride coating in rats. The MgF<sub>2</sub> layer was prepared on the surface of AZ31 magnesium alloy in saturated NH<sub>4</sub>HF<sub>2</sub> solution by microarc fluorination (MAF) at 190 V. The cross-sectional SEM, EDS, and XRD analysis indicated that the alloy surface was covered with MgF<sub>2</sub>. Meanwhile, SEM observation was used to compare the magnesium alloy samples before and after treatment, and it was found that the samples after coating were flatter and smoother. Two sets of experiments were carried out with the subjects, 6-week-old male rats. So that the untreated AZ31 samples and the microarc fluorinated AZ31 samples could be buried under the muscle layer individually. The volume changes and surface morphology of the corroded samples were monitored dynamically using micro-CT over a 16-week period *in vivo*. Comparison of results between the two sets of samples presented that the corrosion of the microarc fluorinated samples was much slower than that of the untreated ones. The MAF coating was shown to be effective in controlling the corrosion rate and progression of the magnesium alloy.

## 1. Introduction

As a biomaterial, magnesium (Mg) and magnesium alloys are promising for medical applications. Magnesium and magnesium alloys provide with high specific strength and desirable biocompatibility as implantable materials. Moreover, the density of magnesium and magnesium alloys is similar to that of the human bone [1, 2]. Nowadays, clinical practice commonly uses materials that primarily provide long-term structural stability, such as cobalt chromium alloys, titanium alloys, stainless steel, and other metals. However, because these materials are alien to the body, allergic or inflammatory reactions during treatment are also very common in subsequent recovery [3]. The process of bone remodeling will also be severely disrupted if a stress shielding effect occurs. Even secondary fractures could occur after implant removal sur-

gery [4, 5]. It is worth noting that secondary surgeries after fracture healing will undoubtedly increase pain and medical costs. Magnesium materials, meanwhile, may avoid the aforementioned side effect. Consequently, magnesium alloy seems to be a more desirable option. Nevertheless, one outstanding drawback of magnesium materials is the rapid corrosion rate in human body. It will lead to problem such as an increase in the osmotic pressure of the local microenvironment, which may decrease the whole mechanical strength [1]. Therefore, it is a standing concern for scholars to control the corrosion rate of magnesium alloy.

The composition modification and alloy surface treatment can be used to slow down the corrosion progress of magnesium alloys. The former can improve its corrosion resistance and mechanical properties but not its bioactivity [6]. Currently, the commonly used surface modification

methods are ionic, carbon treatment, fluoride treatment, etc. At this stage of research, electrochemical corrosion analysis has demonstrated that the magnesium fluoride ( $\text{MgF}_2$ ) layer can increase the polarization resistance of magnesium alloys [7–9]. In addition, in the existing studies to prove that the preparation of  $\text{MgF}_2$  coating has a certain influence on the corrosion resistance [7, 10, 11]. In addition, the biocompatibility of the  $\text{MgF}_2$  coatings has been shown to be positive in cytotoxicity experiments. The negative effects of the magnesium alloy on the degradation and precipitation of hydrogen gas in body fluids have been mitigated to some extent [8, 12, 13]. A point of interest is that the antimicrobial action of the magnesium fluoride coating is another property that has been found in previous studies [3]. In corrosion experiments, the  $\text{Mg}^{2+}$  and  $\text{F}^-$  ions produced during the degradation of the alloy are not only nontoxic to the surrounding tissues but also have a nutritional effect on the formation of the bone [6]. Fluorine in bone tissue mediates the metabolism of calcium and phosphorus and helps build bone strength [14]. Mg alloys coated with  $\text{MgF}_2$  are highly resistant to corrosion *in vivo*. Additionally, its anticorrosive ability can be controlled to meet the requirements for implant retention for an appropriate period of time. The sustainability of the  $\text{MgF}_2$  coating is evident.

Experiments have been carried out to prepare  $\text{MgF}_2$  coatings using the microarc fluorination (MAF) method [15–17]. A series of *in vitro* corrosion tests proved that the microarc fluoride treated magnesium alloy, compared to the untreated ones, has been significantly improved in anticorrosion properties. Moreover, the proliferation and adhesion rates of cells grown on the coating were advanced [15, 16]. This method is based on the principle of electrolysis.  $\text{MgF}_2$  layers are prepared on magnesium or magnesium alloy substrates using a certain voltage as a reaction condition in a fluorinated solution [17, 18]. The MAF method was followed in this experiment. The purpose of this work is to observe the corrosion control by the MAF coating under the rat-body-fluid environment. A 190 V volt-treated MAF coating was prepared, and its dynamic changes and degradation behavior were recorded inside the experimental subjects. Its pre- and post-corrosion morphology, composition, and corrosion resistance were evaluated. This study complements the experiment system for the preparation of microarc fluorinated magnesium fluoride coatings by *in vivo* experiments.

## 2. Materials and Methods

**2.1. Materials and Pretreatment.** In this study, the size of the AZ31 (Dongguan FeiTai Metal Products Co., Ltd., China) was approximately 70.0 mm [3]. Then, polish the casted samples to 1000 grids. The AZ31 chemical composition is indicated in Table 1.

The testing samples were treated with microarc fluorination (MAF) method. Fluorinated coatings were prepared on samples in saturated  $\text{NH}_4\text{HF}_2$  solution using 190 V constant voltage DC mode. A closed circuit was formed with AZ31 as anode and graphite rod as cathode during electrification. Clean all the samples with distilled water three times and

TABLE 1: Chemical composition of AZ31 (mass fraction, %).

Al	Zn	Mn	Si	Mg
2.87	0.85	0.38	0.1	Balance

dried thoroughly. The samples were divided into two groups labeled “Bare” and “MAF.”

**2.2. Coating Observation.** The morphology and cross-sectional images of each surface of the sample were observed by scanning electron microscopy (specific model reference: FE-SEM, JSM-67000). Then, the basic composition was determined by the energy spectrometer (EDS). The Mg phases on the surface of  $\text{MgF}_2$  samples were measured at 40 kV and 30 mA by X-ray diffraction (XRD, Rigaku Ultima IV Japan), and the scan rate was 1/min.

**2.3. Electrochemical Experiment.** The Potential Dynamic Polarization (PDP) tests were performed with a constant potentiostat (VersaSTAT 3: 300) and commercial software (VersaStudio 2.44.). The electrochemical analysis cell included a classical three-electrode cell which contained the testing sample as a working electrode, a pure platinum rod electrode, and a reference electrode (Ag/AgCl/Sat-KCl+197 mV vs. standard hydrogen electrode). Here, 1000 mL of commercial Hank’s Balanced Salt Solution (HBSS) solution (WELGENE Inc., Korea) was used as the electrolyte and placed in a double-walled beaker. Maintain the temperature of the electrolyte at  $37 \pm 1^\circ\text{C}$  using a recirculating water heater. The scanning rate of PDP measurements was 3 mV/s.

### 2.4. Animal Experiments

**2.4.1. Experimental Design.** *In vivo* experiments were conducted with respect for animal ethics and animal protection guidelines. Six 6-week-old male rats (New Zealand) with an average weight of 180 g were randomly selected for this study. The rats were divided into two groups; one group was experimented with the Bare, and the other group was experimented with the MAF. After 16 weeks, the rats were euthanized, and the samples were removed.

**2.4.2. Surgical Procedures.** Firstly, the rats were anesthetized with isoflurane (Isolurane inhalation anesthetic solution; Pizer Japan Inc., Tokyo, Japan). Peel off the skin, fascia to expose the anterior tibial muscle. A sample was buried between the right tibial muscle and periosteum by dental round-bar and a nontaper tissue bar. Then, press the implant and flushed with saline, which can be seen in Figure 1. The wound was closed by suture needle (Nylon suture 5-0; Natsume seisakusho Co., Ltd.). After suturing the incision, put the rat on the pad until they recovered from the anesthetic state. For postoperative analgesia, 0.5 mL of transaminopurine hydrate (sulpyrine injection 250 mg NP; Nipro Pharma Corporation, Osaka, Japan) was added to in rats’ drinking water as anti-inflammatory and analgesic for two weeks. At the end of the experiments, the rats were anesthetized with

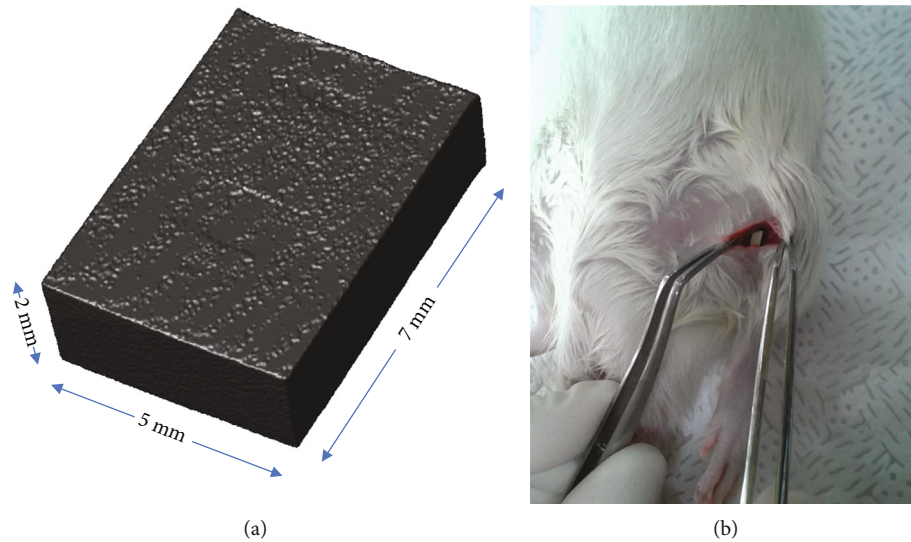


FIGURE 1: In vivo corrosion control samples and intraoperative diagrams in rats. (a) Stereoscopic imaging of the sample and annotation of the sampling size. (b) Preparation of an in vivo corrosion model in rats and surgical burial of the sample.

isoflurane (Pizer Japan Inc.) and euthanized by inhalation of  $\text{CO}_2$ . The samples were removed from each rat.

**2.5. Corrosion Analysis In Vivo.** Samples from the fourth week were scanned by micro-CT (SkyScan1076, Bruker). The micro-CT scanner was set up with 100 kV voltage, 100  $\mu\text{A}$  current, 360-degree rotation, and 17.6  $\mu\text{m}$  pixel size. After the rats were anesthetized, the scan started 1 cm above the implant and ended 1 cm below it. After removal of the samples at week 16, the samples were scanned again. Both the images (2D and 3D) and the volume data were obtained by the program (CTAn-CTVol 1.10).

The volume loss percentages were calculated as:

$$\text{Volume loss\%} = \frac{V_1 - V_2}{V_1} \times 100\%. \quad (1)$$

$V_1$  is the volume before implantation, and  $V_2$  is the volume after 16 weeks. In order to better visualize the *in vivo* morphology at week 16, the samples were washed in chromic acid ( $\text{H}_2\text{CrO}_3$ ) and dried. The surface was observed by SEM.

### 3. Results

**3.1. Specimen Surface Morphology.** Figure 2 illustrates the surface morphology of the MAF group under scanning electron microscopy before it was placed in the body. The surface of  $\text{MgF}_2$  coating was uneven and porous, coral-like.

Figure 3 presents the XRD curves of the Bare and the MAF sampling groups. Comparison of the untreated with the JCPDS standard card indicates that the coating of the treated sample consists of quadrilateral  $\text{MgF}_2$  (JCPDS No. 41-1443) mainly. EDS analysis showed that the coating surface was dominated by F and Mg elements, which accounted for 61.04% and 38.41%, respectively, as shown in Figure 4.

Figure 5 gives the SEM scan of the cross-section of the MAF group. From Figure 5(a), it can be seen that a layer

appeared between the Mg alloy substrate and PMMA, i.e., on the surface of the base. According to the EDS mapping analysis, F elements were only distributed in the upper layer of the samples (Figure 5(c)), averaging 4.26  $\mu\text{m}$  thick. The middle part of the coating was more evenly spaced. The density of fluorine elements decreased as closer to the substrate, and the Mg elements in this depth were relatively sparsely distributed compared to the deeper part (Figure 5(d)). A combination of Figures 5(c) and 5(d) reveals a simultaneous distribution of Mg and F in this domain.

**3.2. Corrosion Experiments.** Figure 6 is the empirical result of the dynamic potential polarization (PDP) experiment. Resistance properties can be reflected by the corrosion potential of the samples ( $E_{\text{corr}}$ ) and the current density ( $I_d$ ). The Bare group showed a corrosion current density of approximately  $4.0 \times 10^{-5}$  A. The  $I_d$  of the MAF group was about  $2.1 \times 10^{-6}$  A, which was about 20 times lower than the former. Significantly better corrosion resistance of the treated specimens can be interpreted.

The surface images obtained by SEM (Figure 7) reveal that the Bare before implantation (Figure 7(a)) was a line shape produced by grinding, whereas the MAF (Figure 7(c)) had a smoother surface view. After removal at week 16, significant pitting was observed on the Bare surface (Figure 7(b)). Scan results displayed a corrosion range of approximately 0.94 mm in diameter. The MAF surface only appeared to be water-washed soil with a few occasional pitting holes, which can be read from Figure 7(d). The surfaces of the Bare were more uneven due to more localized corrosion in comparison.

**3.3. Micro-CT Scanning.** Figure 8 depicts the imaging of two groups of samples *in vivo* at week 4 using micro-CT. The large gas cavity was clearly visible in the Bare group at the location indicated (Figure 8(a)), and there were more small gas cavities around the sample, so that the color spots were

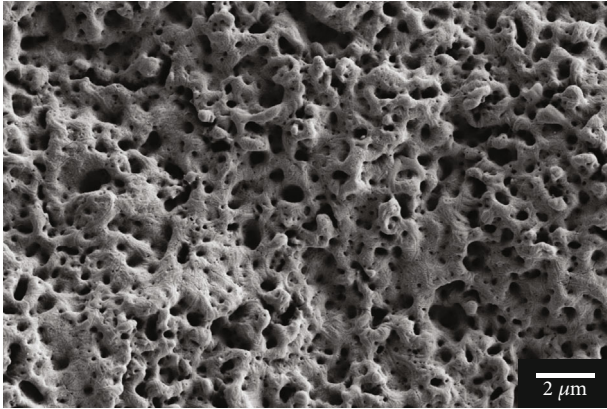


FIGURE 2: FE-SEM observing surface morphology after MAF coated.

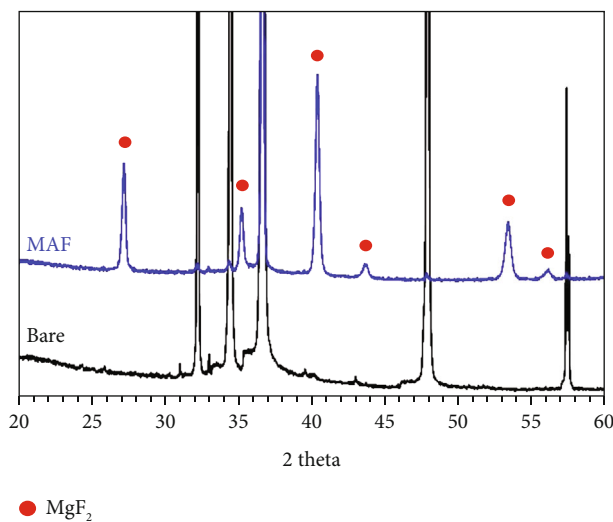


FIGURE 3: XRD patterns of the Bare and the MAF.

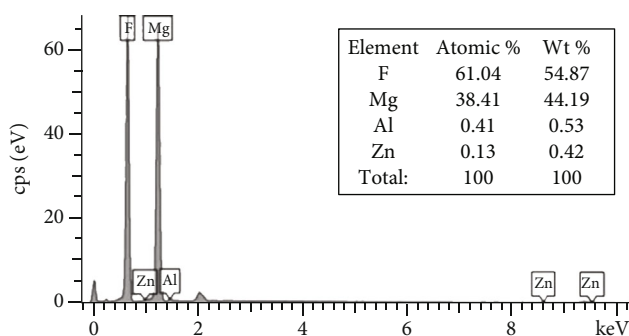


FIGURE 4: EDS spectra of the MAF coating and percentage of element composition.

sparse. The MAF group, on the other hand, had denser imaging around the sample, proving that the gas production was pretty slow.

Figure 9 contains the results of micro-CT imaging of the specimens at weeks 0, 4, and 16, respectively. At week 4, a corrosion pit appeared in the lower left corner of the Bare samples and tended to enlarge. At 16 weeks, the sampling

from the Bare group had other corrosion pits in addition to the one in the lower left corner, the largest of which was nearly 1 mm in diameter. In addition to this, it can be noted that the rectangular form becomes incomplete. Nevertheless, the MAF group had only a few pitting-like indentations on the surface of the sample. Judging from the results of week 4 and week 16, the MAF group would be less corrosive than the Bare group no matter what.

Figure 10 is a histogram produced from the volume loss after sample removal. The volume loss in the Bare group was 14.9% compared to 3.2% in the MAF group. The Bare group was approximately 4.67 times more likely to be in the MAF group.

#### 4. Discussion

Mg alloy, as a biodegradable biomaterial, is commonly used to provide short-term support during tissue recovery, and its potential for medical applications is recognized [19–22]. Nevertheless, it has been demonstrated in existing studies that the rapid degradation rate and localized corrosion behavior of magnesium alloys hinder their clinical application [23, 24]. The existing problems may lead to a mismatch between the support period and the tissue recovery process or even fracture damage to the implant due to stress concentration [8, 25, 26]. In order to solve the fundamental problem, controlling the corrosion rate of magnesium alloys in the electrolyte *in vivo* has become a more widely studied objective.

Surface coating treatment of magnesium alloys has been used in many studies, and effective corrosion rate mitigation results have been obtained. The surface modification treatment can also improve the biocompatibility of magnesium alloys as biomaterials [8]. It is worth mentioning that the coating treatment used should satisfy the following points: (I) strong adhesion to magnesium alloy substrate, (II) provide corrosion resistance, and (III) no cytotoxicity. In addition, for stable degradation of the material within the physiological environment, the corrosion products should also have good biocompatibility assessment results [27]. Li et al. [28] found that Mg fluoride coating in 3.5% NaCl solution improved the bioactivity of the samples. Chiu et al. [29] conducted experiments using HBSS solution and found that MgF<sub>2</sub> coating improved the corrosion resistance of the samples.

The corrosion tests in the *in vivo* environment were performed in combination with existing *in vitro* experiments on the MAF coating treatment. The composition, surface morphology, and electrochemistry of MAF-coated magnesium alloys have been evaluated to some extent by *in vitro* experiments in previous studies, with more satisfactory results [15–17]. In this experiment, the processed AZ31 samples were processed at 190 V constant voltage mode. Figure 2 shows the rough coral-like surface morphology of the microarc fluoride treated magnesium alloy, similar to previous MAF coatings at high voltages [15, 16, 30]. Figure 5(a) shows that the fluoride coating with a thickness of 4.26 μm is evenly distributed on top of the magnesium substrate. The distribution of oxygen elements throughout the section in Figure 5(b) is,

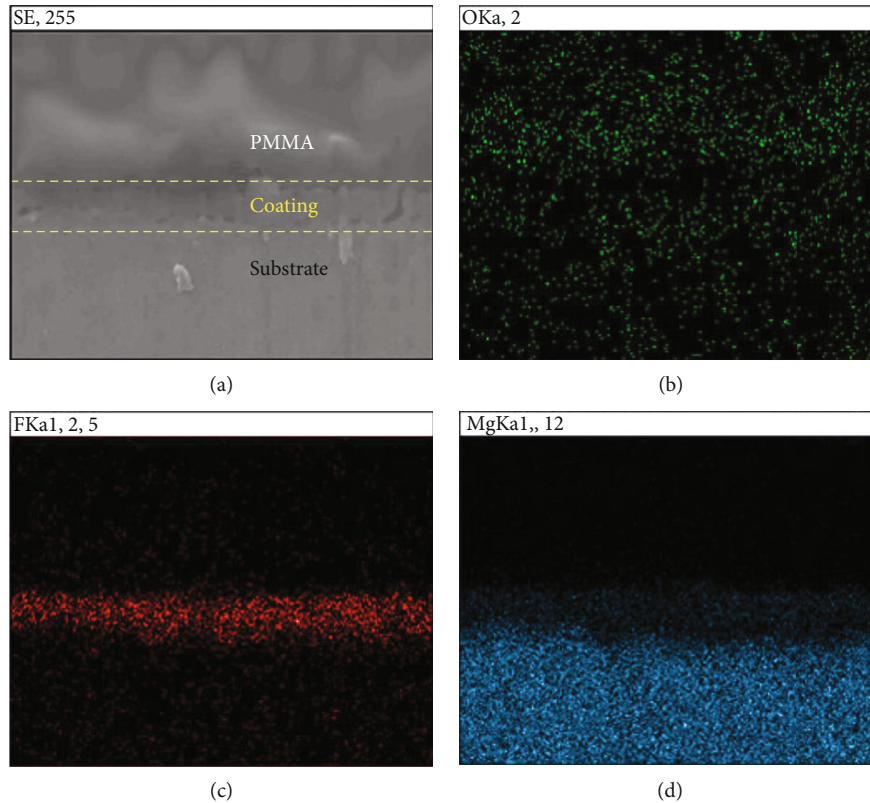


FIGURE 5: Cross-sectional electron microscopy images and energy diffraction spectra of the MAF coating. (a) Cross-sectional morphology observed under the SEM. Cross-sectional elemental mapping assay of the coating by EDS. (b–d) The results of the distribution of the three elements, oxygen, fluorine, and magnesium, respectively.

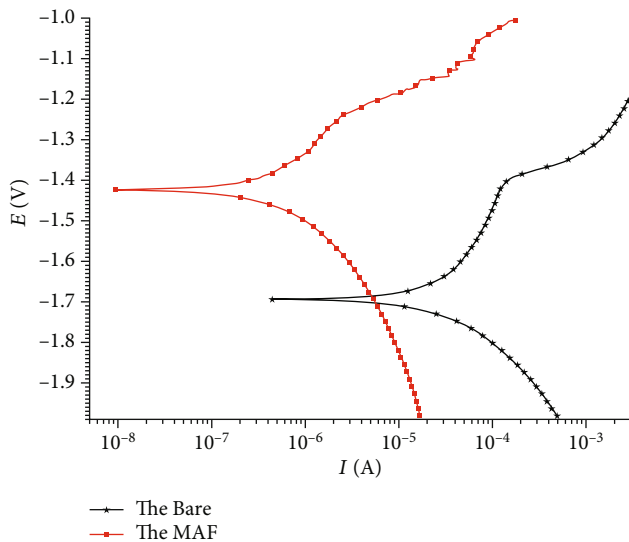


FIGURE 6: Potentiodynamic polarization curves of the Bare and the MAF samples.

we speculated, due to the internal magnesium exposure caused by the casting and grinding. Oxidation reactions with the air will form a thin oxide film. Because of the short reaction time, there is not much oxygen content. By the infiltrative distribution of fluorine elements in Figure 5(c), it can

be assumed that the surface of the substrate is transformed into a fluorinated layer during the electrochemical process. As the fluoride layer grows inward and outward simultaneously, the geometry of the magnesium alloy slightly changes [5]. This also leads to a relative decrease in the distribution density of magnesium in the part of the coating in contact with the substrate. The chemical reaction leads to the combination of magnesium and fluorine atoms, which changes the original distribution of the elements. In addition, the corrosion current density and corrosion potential of the postcoated samples are analyzed by PDP experiments. A significant enhancement of the corrosion resistance can be observed.

Based on the above facts, it can be stated that the coating on the magnesium substrate is prepared completely and that the coating has a certain corrosion limitation. However, the corrosion resistance of MAF-treated coatings in the *in vivo* environment has not been studied previously [15–17]. In a study by Chan [31], the need for loss analysis of implantable materials, especially magnesium alloys, is raised. Fischerauer et al. [32] stated that the surface morphology can affect the corrosion rate to some extent. The use of micro-CT to monitor the corrosion characterization of samples in a body fluid environment is used to determine corrosion behavior and corrosion rate. This allows assessment of the effectiveness of the coating treatment. A certain degree of sample contact damage is avoided, ensuring the accuracy of the scan results.

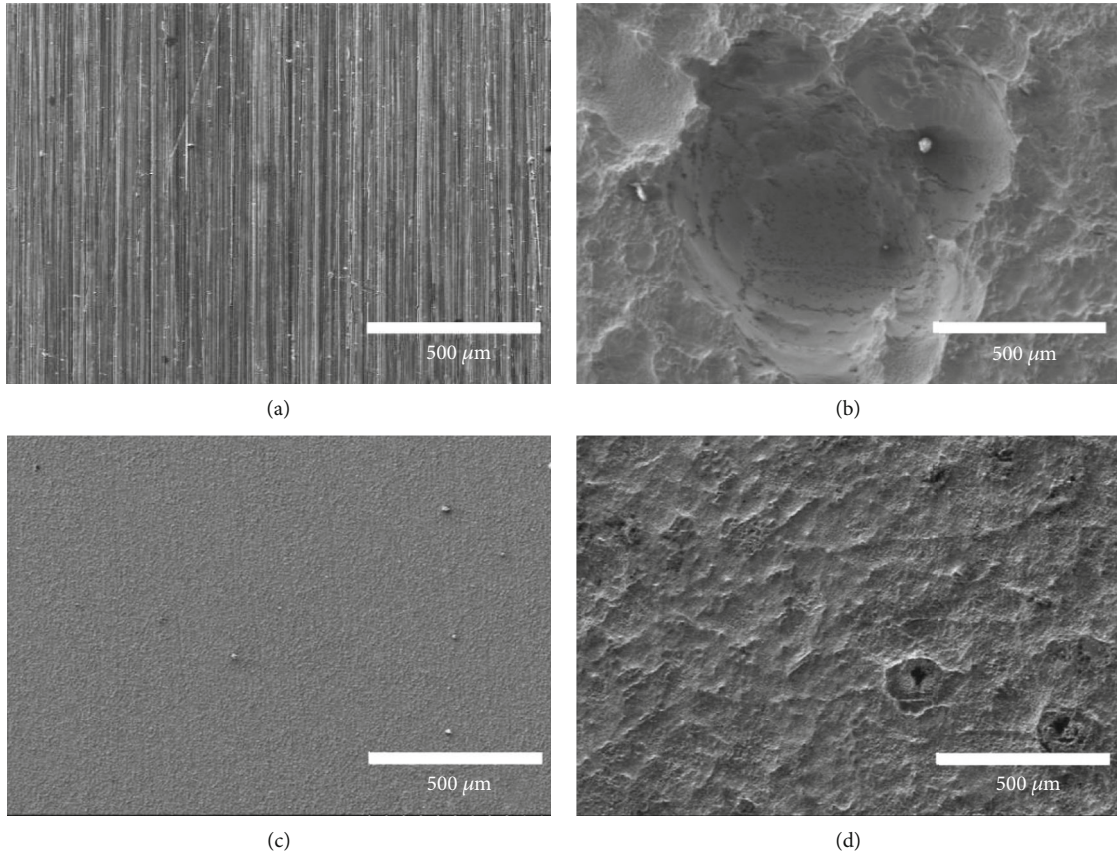


FIGURE 7: Observations of in vivo experimental samples before and after corrosion using FE-SEM. Surface morphology of (a) Bare, 0 week; (b) Bare, 16 weeks; (c) MAF, 0 week; and (d) MAF, 16 weeks.

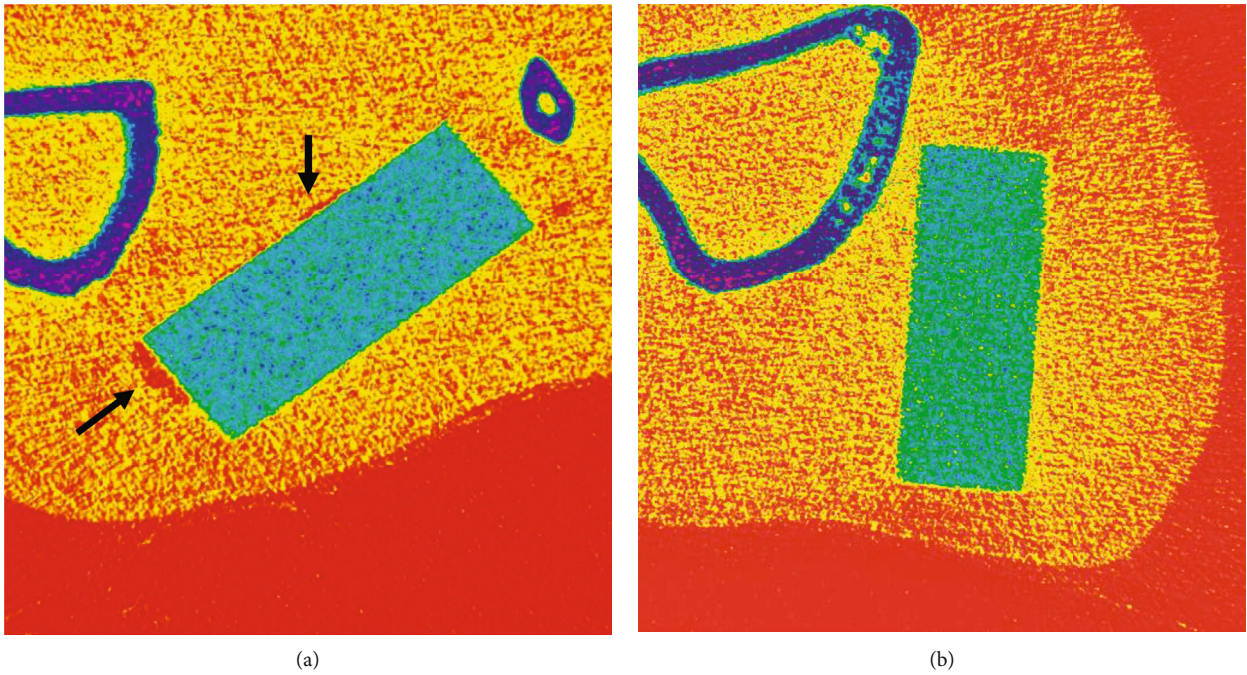


FIGURE 8: 2D results of the micro-CT scan of the sample (a) Bare and (b) MAF burial site at week four.

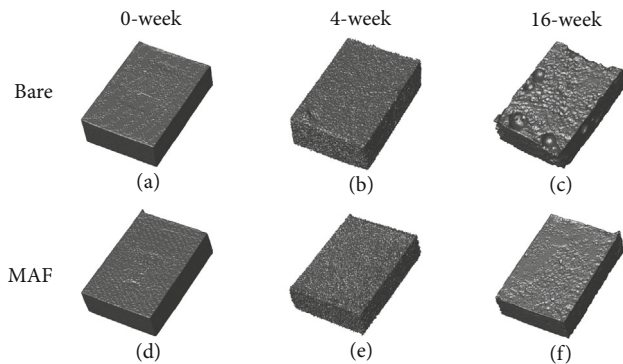


FIGURE 9: Micro-CT scans of samples from in vivo experimental procedures at selected time points, 3D images.

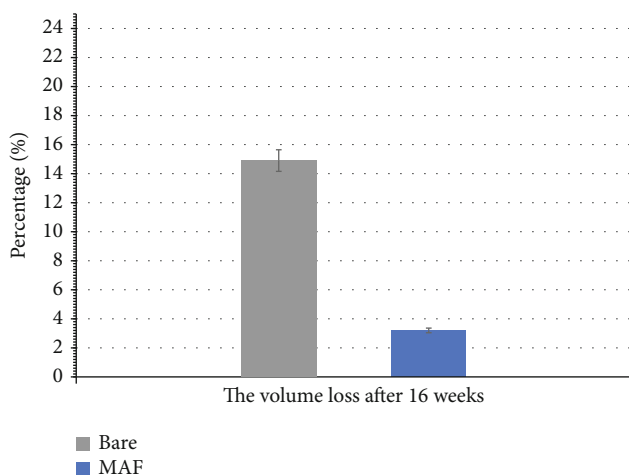
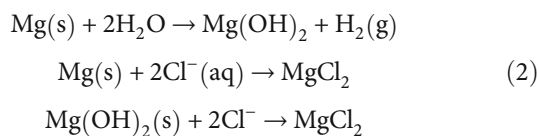


FIGURE 10: Volume change of in vivo experiments.

Magnesium alloys degrade rapidly in a body fluid environment, producing gases, composed mainly of hydrogen [23]. The process is influenced by the complex dynamics of the liquid environment in the organism. It has been shown that the presence of chloride ions ( $\text{Cl}^-$ ) makes the surface of Mg alloys more likely to exhibit the rapid pitting corrosion. Because the body fluid contains a large amount of  $\text{Cl}^-$ , it can be converted into magnesium chloride ( $\text{MgCl}_2$ ) by replacement reaction after contact with magnesium hydroxide formed on the surface of magnesium alloy [23, 33].

In summary, the chemical equation of the reaction is as follows:



Obviously, there is a dynamic exchange of fluids between tissues, and their flow accelerates the corrosion process. It is worth mentioning that the damage of hydrogen bubbles to implants, such as causing a loss of mechanical integrity, has also been reported recently [34]. From

the micro-CT imaging results (Figure 8(a)), it is evident that gas density belts appear around the untreated specimen. The presence of air cavities on the sample contact surface with body fluids represents the occurrence and product accumulation of the anodic dissolution process. This partly reflects the inappropriate degradation rate of magnesium alloys and the difficulty of wound healing due to bubbles. Although bubbles can adversely affect the implant, no further damage to the bone and surrounding tissues was observed, the same as in the subcutaneous magnesium implantation experiments of Kuhlmann et al. [35]. It has been shown that the hydrogen produced during the corrosion of magnesium-based materials can be removed and excreted to some extent [32, 36]. In a sense, the negative effects of corrosion behavior and bubbles can be minimized if the corrosion rate is kept within a safe range [25].

Fluorinated coatings have exhibited desirable properties in many previous studies. In addition to the most common aspects, its antimicrobial properties have been a noteworthy part of the research process since 1940 [37, 38]. Materials with bacterial resistance are highly desirable in medical implantation procedures [8, 39]. Scanning electron microscopy observation of the MAF coating in this experiment reveals similarities between the fluorinated coating and the previous study [15–17]. Therefore, we compared the results of the *in vivo* corrosion with the Hank's Balanced Salt Solution (HBSS) immersion experiments from previous studies. Similarities in the corrosion traces could be found [15–17]. Observation of Figure 9 SEM scan reveals an obvious corrosion pit, indicating localized corrosion of the uncoated magnesium alloy in a body fluid environment. This implies that corrosion does not develop uniformly at the interface between the alloy and the body fluid. Conversely, site-directed degradation corrosion has occurred at certain locations, and the corrosion process at that location is more advanced than at other planes at the same depth [40, 41]. When the rate of corrosion is greater than the carry-over excretion of body fluids, the gas accumulates and creates cavities. In other words, there is a high probability of gas localization at the location of the corrosion pits. This can also be demonstrated in conjunction with Figures 7(b) and 8(a). It can be inferred from the above facts that the presence of the  $\text{MgF}_2$  coating not only reduces the contact area between the magnesium alloy and body fluids but also effectively inhibits the rate of  $\text{H}_2$  production and reduces the damage of the implant material itself.

## 5. Conclusion

In this experiment, magnesium fluoride coatings were prepared on the surface of AZ31 magnesium alloy at 190 V constant voltages and evaluated for *in vivo* corrosion experiments, the following conclusions can be drawn.

- (1) Homogeneous and dense magnesium fluoride coatings are prepared and bonded to the magnesium alloy substrate

- (2) *In vitro* corrosion tests showed that the coating could significantly improve the corrosion resistance compared to bare magnesium alloy
- (3) *In vivo* experiments in rats showed that the coating provided protection to the magnesium alloy and significantly reduced gas generation and accumulation during the corrosion process. 190 V MAF coating exhibits good corrosion resistance in an *in vivo* environment

The combined results demonstrate that the MgF<sub>2</sub> coating is effective in controlling the corrosion rate and progression of magnesium alloys, which shows its potential for medical implant material.

### Data Availability

The data used to support findings of this study are included within the article.

### Conflicts of Interest

We declare that we have no financial and personal relationships with other people or organizations that can inappropriately influence our work.

### Authors' Contributions

Xinzhe Gao, Chun Yu Dai, and Qi Jia contributed equally to this work.

### Acknowledgments

This study was funded by the Shandong Medicine & Health Science Technology Development Plan Project (2018WS125) and the Tai'an Science & Technology Development Plan Project (2019GX043).

### References

- [1] L. Y. Li, L. Y. Cui, R. C. Zeng et al., "Advances in functionalized polymer coatings on biodegradable magnesium alloys - a review," *Acta Biomaterialia*, vol. 79, pp. 23–36, 2018.
- [2] Y. Su, J. Lin, Y. Su, W. Zai, G. Li, and C. Wen, "Investigation on composition, mechanical properties, and corrosion resistance of Mg-0.5Ca-X(Sr, Zr, Sn) biological alloy," *Scanning*, vol. 2018, Article ID 6519310, 10 pages, 2018.
- [3] M. P. Staiger, A. M. Pietak, J. Huadmai, and G. Dias, "Magnesium and its alloys as orthopedic biomaterials: a review," *Biomaterials*, vol. 27, no. 9, pp. 1728–1734, 2006.
- [4] J.-H. Kim, M.-S. Kook, S.-Y. Ryu, H.-K. Oh, and H.-J. Park, "A simple technique for the treatment of inferior orbital blow-out fracture: a transantral approach, open reduction, and internal fixation with miniplate and screws," *Journal of Oral and Maxillofacial Surgery*, vol. 66, no. 12, pp. 2488–2492, 2008.
- [5] H. Hornberger, S. Virtanen, and A. R. Boccacini, "Biomedical coatings on magnesium alloys – a review," *Acta Biomaterialia*, vol. 8, no. 7, pp. 2442–2455, 2012.
- [6] H. Jiang, J. Wang, M. Chen, and D. Liu, "Biological activity evaluation of magnesium fluoride coated Mg-Zn-Zr alloy *in vivo*," *Materials Science & Engineering C: Materials for Biological Applications*, vol. 75, pp. 1068–1074, 2017.
- [7] H. R. Bakhsheshi-Rad, M. H. Idris, and M. R. Abdul-Kadir, "Synthesis and *in vitro* degradation evaluation of the nano-HA/MgF<sub>2</sub> and DCPD/MgF<sub>2</sub> composite coating on biodegradable Mg-Ca-Zn alloy," *Surface & Coatings Technology*, vol. 222, pp. 79–89, 2013.
- [8] T. Yan, L. Tan, B. Zhang, and K. Yang, "Fluoride conversion coating on biodegradable AZ31B magnesium alloy," *Journal of Materials Science & Technology*, vol. 30, no. 7, pp. 666–674, 2014.
- [9] T. Yan, L. Tan, D. Xiong, X. Liu, B. Zhang, and K. Yang, "Fluoride treatment and *in vitro* corrosion behavior of an AZ31B magnesium alloy," *Materials Science and Engineering*, vol. 30, no. 5, pp. 740–748, 2010.
- [10] M. Ren, S. Cai, T. Liu, K. Huang, and X. Wu, "Calcium phosphate glass/MgF<sub>2</sub> double layered composite coating for improving the corrosion resistance of magnesium alloy," *Journal of Alloys and Compounds*, vol. 591, pp. 34–40, 2014.
- [11] J. H. Jo, B. G. Kang, K. S. Shin et al., "Hydroxyapatite coating on magnesium with MgF<sub>2</sub> interlayer for enhanced corrosion resistance and biocompatibility," *Journal of Materials Science Materials in Medicine*, vol. 22, no. 11, pp. 2437–2447, 2011.
- [12] X. Liu, Z. Zhen, J. Liu et al., "Multifunctional MgF<sub>2</sub>/Polydopamine coating on Mg alloy for vascular stent application," *Journal of Materials Science & Technology*, vol. 31, no. 7, pp. 733–743, 2015.
- [13] Z. Li, S. Shizhao, M. Chen, B. D. Fahlman, D. Liu, and H. Bi, "*In vitro* and *in vivo* corrosion, mechanical properties and biocompatibility evaluation of MgF<sub>2</sub>-coated Mg-Zn-Zr alloy as cancellous screws," *Materials Science & Engineering C: Materials for Biological Applications*, vol. 75, pp. 1268–1280, 2017.
- [14] S. Liu, H. Zhou, H. Liu, H. Ji, W. Fei, and E. Luo, "Fluorine-contained hydroxyapatite suppresses bone resorption through inhibiting osteoclasts differentiation and function *in vitro* and *in vivo*," *Cell Proliferation*, vol. 52, no. 3, article e12613, 2019.
- [15] H. B. Jiang, Y. K. Kim, J. H. Ji, I. S. Park, T. S. Bae, and M. H. Lee, "Surface modification of anodized Mg in ammonium hydrogen fluoride by various voltages," *Surface & Coatings Technology*, vol. 259, pp. 310–317, 2014.
- [16] H. B. Jiang, G. Wu, S.-B. Lee, and K.-M. Kim, "Achieving controllable degradation of a biomedical magnesium alloy by anodizing in molten ammonium bifluoride," *Surface and Coatings Technology*, vol. 313, pp. 282–287, 2017.
- [17] J. Sun, S. Jin, B. C. Zhao et al., "Enhanced corrosion resistance of biodegradable Mg alloys via ultrasonically treated fluoride coating," *Surface Topography: Metrology and Properties*, vol. 7, no. 2, article 025009, 2019.
- [18] L. Sun, B. C. Zhao, T. Wang et al., "Surface characterization and corrosion resistance of biomedical AZ31 Mg alloy treated by microarc fluorination," *Scanning*, vol. 2020, Article ID 5936789, 15 pages, 2020.
- [19] F. Witte, V. Kaese, H. Haferkamp et al., "In vivo corrosion of four magnesium alloys and the associated bone response," *Biomaterials*, vol. 26, no. 17, pp. 3557–3563, 2005.
- [20] X. Guan, M. Xiong, F. Zeng et al., "Enhancement of osteogenesis and biodegradation control by brushite coating on Mg-Nd-Zn-Zr alloy for mandibular bone repair," *ACS Applied Materials & Interfaces*, vol. 6, no. 23, pp. 21525–21533, 2014.
- [21] C. Castellani, R. A. Lindtner, P. Hausbrandt et al., "Bone-implant interface strength and osseointegration: biodegradable

- magnesium alloy versus standard titanium control,” *Acta Biomaterialia*, vol. 7, no. 1, pp. 432–440, 2011.
- [22] L. Mao, L. Shen, J. Chen et al., “Enhanced bioactivity of Mg–Nd–Zn–Zr alloy achieved with nanoscale MgF<sub>2</sub> surface for vascular stent application,” *ACS Applied Materials & Interfaces*, vol. 7, no. 9, pp. 5320–5330, 2015.
- [23] L. Mao, H. Zhou, L. Chen et al., “Enhanced biocompatibility and long-term durability in vivo of Mg–Nd–Zn–Zr alloy for vascular stent application,” *Journal of Alloys and Compounds*, vol. 720, pp. 245–253, 2017.
- [24] Y. Chen, Z. Xu, C. Smith, and J. Sankar, “Recent advances on the development of magnesium alloys for biodegradable implants,” *Acta Biomaterialia*, vol. 10, no. 11, pp. 4561–4573, 2014.
- [25] C. M. Weber, R. Eifler, J. M. Seitz et al., “Biocompatibility of MgF<sub>2</sub>-coated MgNd<sub>2</sub> specimens in contact with mucosa of the nasal sinus – a long term study,” *Acta Biomaterialia*, vol. 18, pp. 249–261, 2015.
- [26] D. Ahmadvhaniha, A. Järvenpää, M. Jaskari et al., “Microstructural modification of pure Mg for improving mechanical and biocorrosion properties,” *Journal of the Mechanical Behavior of Biomedical Materials*, vol. 61, pp. 360–370, 2016.
- [27] T. N. Rezukhina, T. F. Siseova, L. I. Holokhonova, and E. G. Ippolitov, “The thermodynamic properties of some metal fluorides solid-electrolyte galvanic-cell studies,” *The Journal of Chemical Thermodynamics*, vol. 6, no. 9, pp. 883–893, 1974.
- [28] J. Li, J. Huang, Y. Tian, and C. Liu, “Corrosion action and passivation mechanism of magnesium alloy in fluoride solution,” *Transactions of Nonferrous Metals Society of China*, vol. 19, no. 1, pp. 50–54, 2009.
- [29] K. Y. Chiu, M. H. Wong, F. T. Cheng, and H. C. Man, “Characterization and corrosion studies of fluoride conversion coating on degradable Mg implants,” *Surface and Coatings Technology*, vol. 202, no. 3, pp. 590–598, 2007.
- [30] K. Saranya, M. Kalaiyaran, S. Chatterjee, and N. Rajendran, “Dynamic electrochemical impedance study of fluoride conversion coating on AZ31 magnesium alloy to improve bioadaptability for orthopedic application,” *Materials and Corrosion*, vol. 70, no. 4, pp. 698–710, 2019.
- [31] L. C. Chan, K. M. Au, and K. M. Yu, “FEM–CT integrated design for multiscale damage analysis of hydroformed magnesium-based alloy tubular product,” *NDT & E International*, vol. 56, pp. 38–47, 2013.
- [32] S. F. Fischerauer, T. Kraus, X. Wu et al., “In vivo degradation performance of micro-arc-oxidized magnesium implants: a micro-CT study in rats,” *Acta Biomaterialia*, vol. 9, no. 2, pp. 5411–5420, 2013.
- [33] G. Song, A. Atrons, D. Stjohn, J. Nairn, and Y. Li, “The electrochemical corrosion of pure magnesium in 1 N NaCl,” *Corrosion Science*, vol. 39, no. 5, pp. 855–875, 1997.
- [34] K. Tesař and K. Balík, “Nucleation of corrosion products on H<sub>2</sub> bubbles,” *Materials Today*, vol. 35, pp. 195–196, 2020.
- [35] J. Kuhlmann, I. Bartsch, E. Willbold et al., “Fast escape of hydrogen from gas cavities around corroding magnesium implants,” *Acta Biomaterialia*, vol. 9, no. 10, pp. 8714–8721, 2013.
- [36] T. Kraus, S. F. Fischerauer, A. C. Hänzi, P. J. Uggowitzer, J. F. Löffler, and A. M. Weinberg, “Magnesium alloys for temporary implants in osteosynthesis: in vivo studies of their degradation and interaction with bone,” *Acta Biomaterialia*, vol. 8, no. 3, pp. 1230–1238, 2012.
- [37] S. Naorungroj, H.-H. Wei, R. R. Arnold, E. J. Swift Jr., and R. Walter, “Antibacterial surface properties of fluoride-containing resin-based sealants,” *Journal of Dentistry*, vol. 38, no. 5, pp. 387–391, 2010.
- [38] J. Lellouche, A. Friedman, J.-P. Lellouche, A. Gedanken, and E. Banin, “Improved antibacterial and antibiofilm activity of magnesium fluoride nanoparticles obtained by water-based ultrasound chemistry,” *Nanomedicine: Nanotechnology, Biology and Medicine*, vol. 8, no. 5, pp. 702–711, 2012.
- [39] C. Liu, Z. Ren, Y. Xu, S. Pang, X. Zhao, and Y. Zhao, “Biodegradable magnesium alloys developed as bone repair materials: a review,” *Scanning*, vol. 2018, Article ID 9216314, 15 pages, 2018.
- [40] W. W. Song, J. H. Heo, J. H. Lee, Y. M. Park, and Y. D. Kim, “Osseointegration of magnesium-incorporated sand-blasted acid-etched implant in the dog mandible: resonance frequency measurements and histomorphometric analysis,” *Tissue Engineering and Regenerative Medicine*, vol. 13, no. 2, pp. 191–199, 2016.
- [41] Y.-J. Lee, Y. Kim, J. Y. Kim, J. B. Huh, M. R. Kim, and S. J. Kim, “Effect of different concentrations of Escherichia coli-derived rhBMP-2 coating on osseointegration of implants in dogs,” *Tissue Engineering and Regenerative Medicine*, vol. 9, no. 4, pp. 209–215, 2012.